Journal of the Iranian Chemical Society (2022) 19:3993–4004
https://doi.org/10.1007/s13738-022-02580-1

ORIGINAL PAPER

The Mn(II), Co(II), Ni(II) and Cu(II) complexes of (*Z*)-*N*′((1H-indol-3-yl) methylene)nicotinohydrazide Schiff base: synthesis, characterization and biological evaluation

Neelufar[1] · Javarappa Rangaswamy[1] · Kariyappa N. Ankali[1] · Nagaraja Naik[1] · Bettadapura Rameshgowda Nuthan[2] · Sreedharamurthy Satish[2]

Received: 4 June 2021 / Accepted: 16 April 2022 / Published online: 19 May 2022

Abstract

Schiff bases being biological moieties possess diverse biological and pharmaceutical applications. Metal ions play an important role in various functions of the biological system as well as the human body. The importance of Schiff base and their metal complexes have been acknowledged in the field of bioinorganic chemistry. The current investigation hence focuses on the synthesis and characterization of a bidentate indole-based ligand(Z)-*N*′((1H-indol-3-yl)methylene)nicotinohydrazide **(L)** derived from indole-3-carboxaldehyde **(1)**, nicotinic acid hydrazide **(2)** and their metal complexes of Mn(II), Co(II), Ni(II) and Cu(II), **(4a–d)** in 2:1 stichiometric ratio. All the synthesized ligand and complexes were characterized by IR, UV–Visible, ^{1}H NMR, ^{13}C NMR, Mass, Powder XRD analysis. Further, the ligand and their metal complexes were screened for antimicrobial, antioxidant and DNA cleavage studies. Among the synthesized complexes, Ni(II) **(4c)** showed highest antimicrobial activity against tested Gram −ve and Gram +ve bacterial strains and fungal microorganism, better than the ligand **(L)**. The antioxidant activity results showed that the metal complexes **(4a–d)** were observed to be more active than the parent ligand. Furthermore, the ligand **(L)** and their respective metal (II) complexes **(4a–d)** were found to cleave the pBR322 DNA, during gel electrophoresis studies.

Keywords Indole · Schiff base · Metal complexes · Antimicrobial · Antioxidant · DNA cleavage · Biological activities

Introduction

The hetero aryl rings which are the potent basic pharmacodynamics nucleus are widely distributed in nature and possess a wide variety of biological properties viz; anti-inflammatory, anticancer, antimicrobial activities. The N-heterocyclic ligand has been of great interest due to its usage in many areas of science such as proton transfer reaction, co-ordination chemistry [1]. To adequately select a ligand, it is important to know its geometric characteristic and its behavior. A library of compounds and their key features is convenient for a better design of the targeted structure [2]. The indole ring is an important hetero aryl moiety in many pharmacologically active compounds. Some of the individual anticancer compounds which contains indole ring is responsible for the activity panabinostat, cedriranib, etc. [3].

Indole moiety is a synthetic member of the statin class of drug used to lower cholesterol and prevent cardiovascular disease. The indole motif is arguably one of the most significant heterocycles since they are found in numerous natural products and bioactive molecules [4]. Many pharmacodynamic compounds containing indole nucleus (Fig. 1) have been reported to possess a wide variety of biological properties, namely, anti-inflammatory [5], anticonvulsant [6], cardiovascular [7], antibacterial [8], COX-2 inhibitor [9] and antiviral [10], antimicrobial [11], anticancer activities[12]. More specifically, several reports describe that indole-2-carbohydrazides and related compounds are endowed with antihistaminic [13], antidepressant [14] and MAO inhibitory activities [15].

✉ Nagaraja Naik
drnaikchem@gmail.com

[1] Department of Studies in Chemistry, University of Mysore, Manasagangotri, Mysore 570006, Karnataka, India

[2] Department of Studies in Microbiology, University of Mysore, Manasagangotri, Mysore 570006, Karnataka, India

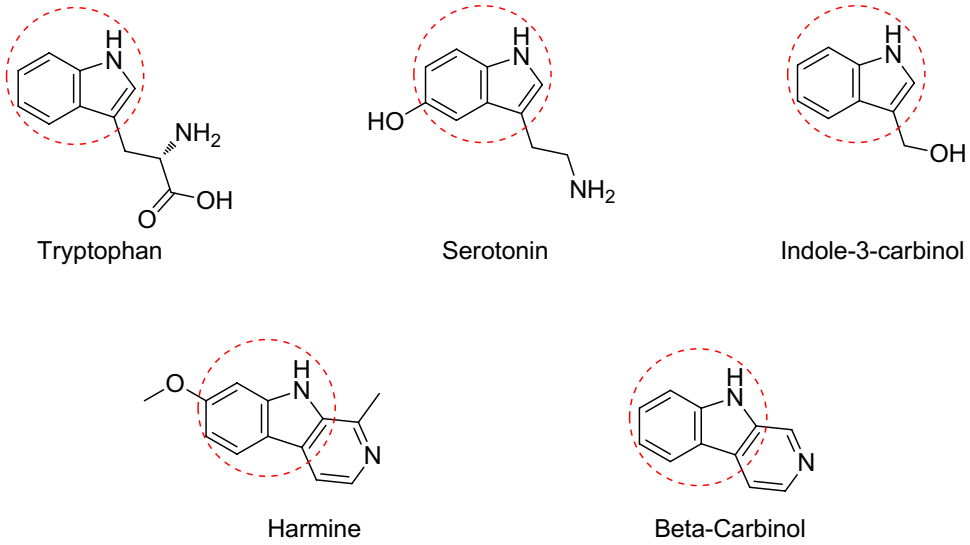

Fig. 1 Some of the biologically active indole derivatives

In addition to this, Schiff base transition metal complexes are very important chelates, and complex assemblies are of great interest from the magnetically point of view [16]. On the other hand, the field of Schiff base complexes has been fast developed because of the wide possible structures for the ligands depending upon the substituted aldehydes and amines considered. Various Schiff bases were reported to possess different genotoxicity [17], antibacterial [18] and antifungal activities [19]. Schiff bases plays a vital role in biological systems, electronic, structural properties as well as their catalytic reduction and pharmaceutical applications [20, 21]. Its metal complexes show interesting and important properties and heavy metal atoms [22] undergoes tautomerism [23] and exhibits catalytic reduction [24, 25] and photochromism [26]. It plays an important role in various chemical and biological process such as stabilizing molecular structures and enzymatic reactions [27]. Generally transition metal complexes that are suitable for binding and cleaving nucleic acids are of significant interest due to their various applications in nucleic acid chemistry like foot printing studies, sequence-specific binding agents and also as a putative anticancer drug [28]. They demonstrated a wide variety of applications in natural sciences such as chemistry, biochemistry and pharmaceutical sciences as well as in the industry [29]. The use of chiral ligands in model complexes has attracted considerable interest for the introduction of chiral information with respect to their catalytic property [30, 31]. Furthermore, these class of complexes act as non-enzymatic models for pyridoxal-amino acid systems, which is a key intermediate in many metabolic reactions of amino acids catalyzed by enzymes which require pyridoxal as a cofactor [32, 33]. Recently, numerous studies have been increasingly devoted to strong hydrogen bonds due to the significant role they play in various fields including proton transfer processes, biochemical reactions and enzyme catalysis [34]. It is expected that N oxidation can increase coordination capacities and flexibility of the ligand together with the enrichment of its properties especially in the selective adsorption and separation gases [35].

Therefore, considering the above facts and in continuation of research interest in the field of bioinorganic and coordination chemistry [36, 37], the present work reports on the synthesis, spectroscopic characterization and biological investigation of Schiff base ligand and its metal complexes Mn(II), Co(II), Ni(II), Cu(II) (Fig. 2).

Experimental section

Materials and methods

Indole-3-carboxaldehyde, nicotinic acid hydrazide and DPPH were purchased from Sigma-Aldrich and used as received without further purification. Metal salts and solvents were obtained from E. Merck and were used without purification. The completion of reaction was monitored by thin layer chromatography (TLC) performed on one coated silica gel plates (MERCK, India). Infrared spectra

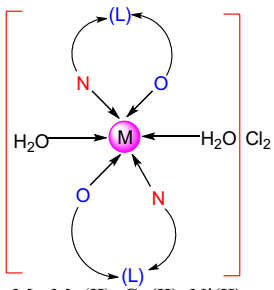

Fig. 2 Structure (*Z*)-*N*′((1H-indol-3-yl)methylene)nicotinohydrazide Schiff base and its metal complexes

were recorded on a Perkin Elmer FT-IR type 1650 Spectrophotometer in the region 4000–400 cm^{-1} using KBr pellets. Mass spectra of synthesized ligand and metal complexes were recorded using a 2010 LC–MS Shimadzu spectrometer. Elemental analysis (C, H, N, O, M) were performed on a Perkin Elmer analytical analyzer. Magnetic susceptibility measurements were performed by the Gouy technique in the solid state at room temperature, and $Hg[Co(NCS)_4]$ is the standard used. TGA analysis was performed on Shimadzu AT-50 thermal analyzer from 25 to 700 °C with a heating rate at 10 °C/min under N_2 atmosphere. The ^1H NMR and ^{13}C NMR spectra were recorded with a variant 400 MHz and 100 MHz DMSO-d_6 as a solvent against tetramethylsilane as an internal standard. Electronic absorption spectra were recorded in the range of 200–800 nm in DMSO using a UV–Visible spectrometer (DU-730 "life science" Beckman coulter, USA). Melting point determination in an open capillary tube using a precision digi melting point apparatus. TGA analysis was performed on a Shimadzu AT-50 thermal analyzer from 30 to 900 °C with a heating rate at 10 °C/min under N_2 atmosphere. The powder X-ray diffraction (PXRD) analysis was carried out at SJCE, Mysuru on a Proto X-ray diffracto meter at 30 kV and 20 mA.

General synthetic procedure

Synthesis of ligand(*Z*)-*N*'-((1H-indol-3-yl)methylene) nicotinohydrazide (L)

An equimolar solution of indole-3-carboxaldehyde (1 mmol) and nicotinic acid hydrazide(1 mmol) in ethanol (5 ml) with a catalytic amount (0.3 ml) of conc. HCl and refluxed at 70 °C for 4 h. Completion of the reaction was monitored using TLC in a n-hexane:ethyl acetate (7:3) solvent system, the obtained yellow precipitate was filtered and washed with cold ethanol. The product was recrystallized using hot ethanol (Scheme 1).

Synthesis of metal complexes 4(a–d)

The ligand **(L)** (2 mmol) was dissolved in hot ethanol with intensive stirring. To this hot suspension, a warm ethanolic solution of $MnCl_2.2H_2O$/ $CoCl_2.6H_2O$/ $NiCl_2.6H_2O$/ $CuCl_2.2H_2O$ (1 mmol) was added drop wise. The resulting mixture was refluxed on a water bath for 5 h at 80 °C. The resulting solid complexes were collected by filtration and washed with ethanol and dried in a vaccume over calcium chloride in a dessicator. (Scheme 2).

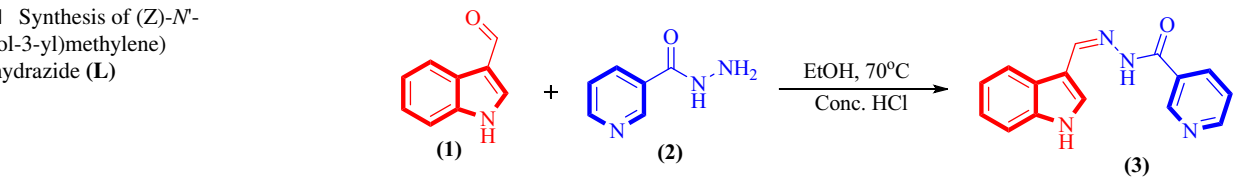

Scheme 1 Synthesis of (Z)-*N*'-((1H-indol-3-yl)methylene) nicotinohydrazide **(L)**

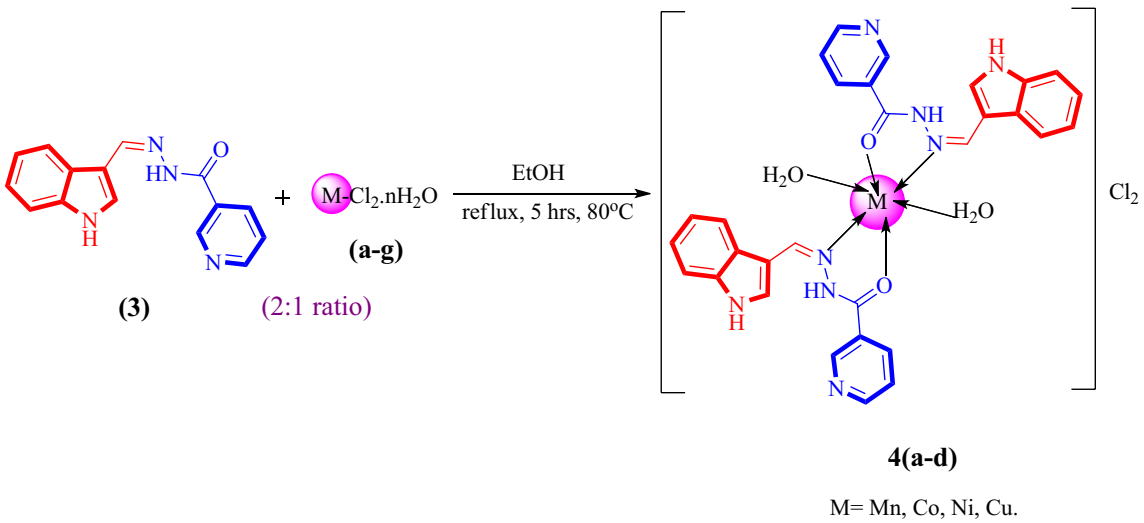

Scheme 2 Synthesis of metal complexes **4(a–d)**

Biological activity

Antimicrobial assay

The synthesized ligand **(L)** and complexes **4(a–d)** were screened for in vitro antimicrobial activity against Gram -ve bacteria as *Escherichia coli* (MTCC 443), *Pseudomonas aeruginosa* (MTCC 2453) and Gram + ve bacterial strains as *Bacillus subtilis* (MTCC 121) and fungal strains *Candida albicans* (ATCC 10,231) and comparison with standard antibiotic ciprofloxacin (25 mg) were served as the positive control. The impact was tested in terms of minimum inhibitory concentration (MIC) using a serial plate dilution assay [38]. Microbial cultures were incubated at 37 °C for a day in the case of bacteria and 72 h for fungi. 100µL of Mueller–Hinton broth of bacteria was pipetted into each well; to this, a 10µL suspension of the test pathogens were then added. 4% DMSO was used as a solvent for solution preparation and served as a negative control in order to monitor sample sterility and to determine any antimicrobial influence of the solvent. Inhibition zone was measured, and MIC was determined using double-fold serial dilution in liquid media containing varying concentrations of test compounds from 1 to 1000 µg/mL. Bacterial growth was measured by the turbidity of the culture after 18 h. Turbidity standard as McFarland Standard 0.5 solution was used. When particular concentration of compound inhibits bacterial growth, half the concentration of the compound was tested. This procedure was carried on to a concentration at which bacteria grow normally. The lowest concentration that inhibits the bacterial growth was determined as MIC value. Three replicates were maintained per test microbe. The resultant MIC values were determined as the mean of these replicate experiments.

Antioxidant activity

Human LDL oxidation assay

Fresh blood was obtained from fasting adult human volunteers and plasma was immediately separated by centrifugation at 1500 rpm for 10 min at 4 °C. LDL (0.1 mg LDL protein/mL) was isolated from freshly separated plasma by preparative ultra-centrifugation using a Beckman L8-55 ultra-centrifuge. The LDL was prepared from the plasma according to the literature method[4]. The isolated LDL was extensively dialyzed against phosphate buffered saline(PBS) pH 7.4 and sterilized by filtration (0.2 µm Millipore membrane system, USA) and stored at 4 °C under nitrogen. 1 mL of various concentrations (10 µM and 25 µM) of the ligand and complexes were taken in test tubes, 40µL of copper sulphate (2 mM) was added, and the volume was made up to 1.5 mL with phosphate buffer (50 mM, pH 7.4). A tube without the compound and with copper sulphate served as a negative control, and another tube without copper sulphate and with compound served as a positive control. All of the tubes were incubated at 37 °C for 45 min. To the aliquots of 0.5 mL drawn at 2, 4 and 6 h intervals from each tube, 0.25 mL of thiobarbutaric acid (TBA, 1% in 50 mM NaOH) and 0.25 mL of trichloro acetic acid (TCA, 2.8%) were added. The tubes were incubated again at 95 °C for 45 min and cooled to room temperature and centrifuged at 2500 rpm for 15 min. A pink chromogen was extracted after the mixture was cooled to room temperature by further centrifugation at 2000 rpm for 10 min. Thiobarbituric acid reactive species in the pink chromogen were detected at 532 nm by a spectrophotometer against an appropriate blank. Data were expressed in terms of malondialdehyde (MDA) equivalent, estimated by comparison with standard graph drawn for 1,1,3,3-tetramethoxy-propane (which was used as standard) give the amount of oxidation, and the results were expressed as protection per unit of protein concentration (0.1 mg LDL protein/mL). Using the amount of MDA, the percentage protection was calculated using the formula: % inhibition of LDL oxidation = (Oxidation in control – oxidation in experimental / oxidation in control) × 100.

DNA Cleavage assay

Agarose-gel electrophoresis monitored the ability of transition metal complexes to cleave plasmid DNA. The experiment was accomplished with supercoiled pBR 322 (200 ng, 1µL) which was treated with varying concentrations of compounds (10–50 µM) in Trisboric acid-buffer with NaCl (50 mM, pH 7.2) by agarose-gel electrophoresis method [39]. The samples (5µLinTris-buffer) were incubated at 37 °C for 45 min in water bath; to this solution, 1µL loading buffer (0.25% bromophenol blue and 30% glycerol) was added. This mixture was loaded in 1% agarose gel, and electrophoresis was carried out at 60 V for an hour. The agarose gel was prestained with 0.5 µg/mL ethidiumbromide (EtBr) and visualized under UV light and photographed for further analysis. The cleavage properties were determined based on the ability of compounds to convert the supercoiled form (FormI) into nicked (FormII) [40].

Results and discussion

Stoichiometry

All the synthesized complexes **(4a–d)** were colored and stable in air, non-hygroscopic, have high melting points and

were insoluble in water, but soluble in coordinating solvents such as DMSO, DMF. The complexes of ligand showed 1:2 (metal:ligand) stoichiometry which was confirmed by elemental analysis and also by spectral studied. The complexes show the composition;

$$\left[M(L)_2(Y)_2\right](X_2)$$

where M = Mn(II), Co(II), Ni(II), Cu(II); X = Cl_2, Y = H_2O.

Electrical conductance measurements

Electrical conductivity measurements are helpful to know whether the anions of the metal salts remain inside or outside the coordination sphere of the central metal atom.

The conductivity measurements in organic solvents for the characterization of coordination compounds have been discussed in detail in a review by Geary [41]. Molar conductance values of different electrolytic systems in different solvents are available as standard references [42].

The molar conductance data (16–55 mhos mol^{-1} cm^{-2}) are presented in Table 1, compared with that of the reported [43] data, which suggested that all metal complexes in 10^{-3} M DMSO were found to be electrolytic in nature, and the anions are not coordinated with metal ions. Thus, it may be concluding that metal complexes of all the anions are present outside the coordination sphere.

Electronic spectra and magnetic moment

The electronic spectral measurement used to assign the possible geometry of the complexes is based on d-d transition peaks. Electronic spectra of ligand **(L)** and its metal complexes **4(a–d)** were measured in DMSO, in the range 200–800 nm and the numerical data are listed in Table 2. The electronic absorption spectrum of the ligand is shown in Fig. 3. The ligand exhibited absorption bands around 260–324 nm. The First and second band around 260 nm corresponds to π-π* of ethane (C=C) bond, the third band at 278 nm corresponds to n-π*transition which indicates that the ligand contains nitrogen group, fourth band around 324 nm corresponds to n-π* transition which indicates the presence of (C=O) group in the ligand moiety. In the metal complexes, π- π* and n- π* transitions were shifted to longer wavelength as a consequence of coordination to metal ion. Besides a moderate broad band found at 368–406 nm with absorption maxima (λmax) at 376 nm (Mn), 369 nm (Co), 372 nm (Ni) and 368 nm (Cu) were attributed to metal–ligand charge transfer (MLCT) transition in complexes (Fig. 4). The spectra further display a broad band in the region 440-550 nm which is due to several metal-centered d-d transitions which may be assigned to d-d transitions of a distorted octahedral geometry, and it may be

Table 1 Molecular formulae, colour, yield, melting point, elemental analysis, and molar conductance data of metal complexes **4(a–d)**

Sl. No	Complexes	Yield (%)	Mel.pt (°C)	Colour	Mol Wt	Elemental analysis Calc. (found) (%)					Ohm^{-1} cm^{-2} mol^{-1}
						M	C	H	N	O	Anion	
1	$[Mn(L)_2(H_2O)_2](Cl_2)$ **(4a)**	82	326	Light brown	618.59	8.40 (8.08)	55.06 (56.14)	3.70 (3.22)	17.12 (16.18)	4.89 (4.79)	10.83 (10.04)	45
2	$[Co(L)_2(H_2O)_2](Cl_2)$ **(4b)**	76	312	Grey	622.48	8.95 (8.96)	54.73 (55.14)	3.67 (3.08)	17.02 (17.01)	4.86 (4.24)	10.77 (10.14)	38
3	$[Ni(L)_2(H_2O)_2](Cl_2)$ **(4c)**	81	306	Brown	622.54	8.92 (8.68)	54.75 (54.93)	3.68 (3.04)	17.03 (16.98)	4.86 (4.46)	10.78 (10.48)	40
4	$[Cu(L)_2(H_2O)_2](Cl_2)$ **(4d)**	78	322	Dark green	591.48	9.59 (9.20)	54.35 (53.75)	3.65 (3.16)	16.90 (16.08)	4.83 (4.08)	10.69 (11.62)	46

Table 2 Electronic spectral data of synthesized ligand **(L)** and its complexes **4(a–d)** along with their absorption band

Sl.No	Complexes	Frequency (cm^{-1})	nm	Absorption and	U_{eff} (BM)	Geometry
1	L	38,461.54 35,971.22–30,864.20	260 278–324	π- π* n- π*	–	–
2	**4a**	26,595.74 20,833.33	376 480	$^6A_{1g} \rightarrow {}^4T_{1g}$ $^6A_{1g} \rightarrow {}^4T_{1g}$	5.62	Octahedral
3	**4b**	27,100.27 18,181.82	369 550	$^4A_2(F) \rightarrow {}^4T_1(F)$ $^4A_2(F) \rightarrow {}^4T_1(P)$	4.38	Octahedral
4	**4c**	26,881.72 18,691.59	372 535	$^1A_{1g}(D) \rightarrow {}^1B_{1g}(G)$ $^1A_{1g}(D) \rightarrow {}^1E_g(G)$	3.36	Octahedral
5	**4d**	27,173.91 19,417.48	368 515	$^2B_{1g} \rightarrow {}^2B_{2g}$ $^2B_{1g} \rightarrow {}^2E_g$	1.85	Octahedral

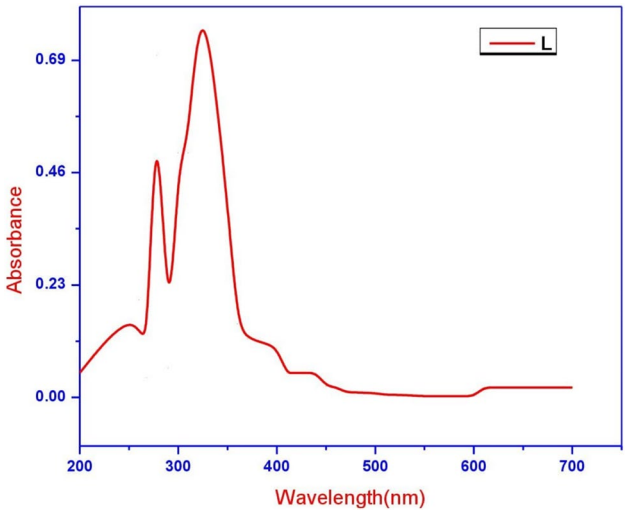

Fig. 3 Electronic spectra of ligand **(L)** and its complexes **4(a–d)**

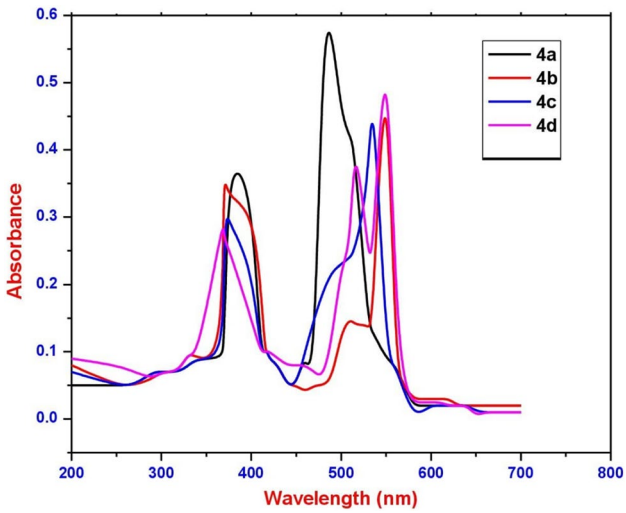

Fig. 4 Electronic spectra of complexes **4(a–d)**

assigned to $^2e_g \rightarrow {}^2t_{2g}$transition. All the complexes exhibited a magnetic moment of 1.85–5.62 BM which is higher than that of the spin-only value [44]. The strong and weak field complexes of some transition metal ions differ in the number of unpaired electrons in the complex, when this number can be ascertained readily from a comparison of the measured magnetic moment and that calculated from the spin paired and spin-free complexes [45]. Determination of the number of unpaired electrons can also give information regarding the oxidation state of a metal ion in a complex. It is also useful in establishing a structure of many complexes [46]. The magnetic susceptibility values of all the complexes **(4a–d)** were predicted in Table 2.

FT-IR spectroscopy

Generally, IR data comparison of the ligand and its metal complexes are of much help to find out which the atoms of the ligand are attached to the metal atom. Attention has been focused on a limited number of bands which provides considerable structural information in order to suggest the most probable manner of coordination of the ligands with metal ions. IR spectrum of the free ligand exhibits a sharp band at 1614 cm^{-1} due to azomethine group vibration and strong band at 3315 cm^{-1} which represents the presence of ν(N–H) group. The strong band at 1552 cm^{-1} ν(C=O) and a medium band at 1124 cm^{-1} can be assigned to ν(N–N) vibrations [47]. This band in complexes is shifted to longer wavelength (lower wavenumber) in the range 1620–1660 cm^{-1} and confirms the coordination of the imine nitrogen to the metal ion. In the spectra of all the complexes, a very broad band at 3091 cm^{-1} is observed signifying the presence of coordinated/lattice held water and N–H stretching frequency observed in the range 3050–3315 cm^{-1}. The bands due to M–O and M–N appeared in the range of 515–540 cm^{-1} and 475–486 cm^{-1}, respectively [48]. The IR data of all the complexes **(4a–d)** were depicted in Table 3. IR spectrum of ligand and complexes are presented in Fig S1–S5.

Table 3 The important infrared frequencies (in cm^{-1}) of the ligand and its metal complexes **4(a–d)**

Sl. No	Code	Complexes	Frequencies (cm^{-1})			
			ν (N–H)	ν (C=N)	ν (M–N)	ν (M–O)
1	**(L)**	L	3315	1614	–	–-
2	**4a**	$[Mn(L)_2(H_2O)_2](Cl_2)$	3310–3286	1660	486	532
3	**4b**	$[Co(L)_2(H_2O)_2](Cl_2)$	3315–3250	1620	475	546
4	**4c**	$[Ni(L)_2(H_2O)_2](Cl_2)$	3298–3255	1634	480	515
5	**4d**	$[Cu(L)_2(H_2O)_2](Cl_2)$	3125–3050	1628	469	540

Table 4 Thermo Gravimetric Analysis metal complexes **4(a–d)**

Complex	Process of degradation	Temp. Range(°C)	Product degradised	No. of moles	Weight	Nature
$[Mn(L)_2(H_2O)_2](Cl_2)$	Dehydration	184–225	H_2O	2	8.35	MnO
	Decomposition of ligand	225–384	Ligand	2	42.81	
	Decomposition of Cl^-	384–568	Cl^-	2	75.33	
$[Co(L)_2(H_2O)_2](Cl_2)$	Dehydration	190–220	H_2O	2	10.20	CoO
	Decomposition of ligand	220–382	Ligand	2	45.20	
	Decomposition of Cl^-	382–560	Cl^-	2	78.40	
$[Ni(L)_2(H_2O)_2](Cl_2)$	Dehydration	175–204	H_2O	2	9.73	NiO
	Decomposition of ligand	204–384	Ligand	2	47.94	
	Decomposition of Cl^-	384–568	Cl^-	2	75.50	
$[Cu(L)_2(H_2O)_2](Cl_2)$	Dehydration	185–222	H_2O	2	11.24	CuO
	Decomposition of ligand	222–375	Ligand	2	46.55	
	Decomposition of Cl^-	375–580	Cl^-	2	81.36	

^{1}H NMR and ^{13}C spectrum of ligand (L)

The ^{1}H NMR spectrum of ligand **(L)** displayed singlet peak at 9.90 ppm which is assigned to CH proton of azomethine group. The ligand also exhibited a singlet peak at 11.96 ppm which corresponds to indole NH proton. The remaining aromatic proton appeared as multiples between 7.12 and 8.82 ppm. The carbon NMR of ligand **(L)** showed azomethine carbon peak at 159.57 (–CH=N), and an aromatic carbon peak appeared in the range 111.8–147.7 ppm. ^{1}H NMR and ^{13}C spectrum of ligand **(L)** are shown in Figs. S6 and S7.

Mass spectra

The LC–MS spectrum of the ligand depicted in Fig. S8 showed a molecular ion peak at m/z-265.12, which is in good agreement with theoretical molecular mass. The mass spectra of complexes showed molecular ion peak for Mn(II), Co(II), Ni(II), Cu(II) complexes **4(a-d)** exhibited m/z 676.57**(4a)**, 622.48**(4b)**, 618.59**(4c)**, 591.48**(4d)**, respectively. Which are coinciding with the stoichiometric composition as the formulae given in Table 1. The LC–MS spectrum of the complexes **4(a–d)** is predicted in Figs. S9–S12.

ThermoGravimetric analysis

Thermal decomposition of all the complexes were carried out to observe the thermal behavior and to determine the decomposition temperature of the complexes. The experimental and calculated TGA data are represented in the Table 4, and TGA curve of complex is presented in Fig. 5.

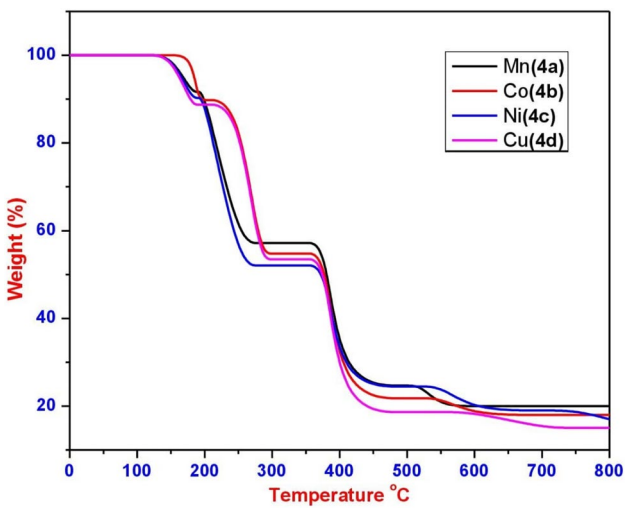

Fig. 5 TGA Curve of synthesized Complexes **(4a–d)**

Table 5 X-ray of $[Ni(L)_2(H_2O)_2]Cl_2$ **(4c)**

Peak No	Observed 2θ	Calculated 2θ	Observed d	Calculated d	hkl	FWHM	Structure
1	11.163	17.082	7.91956	5.18654	0–22	0.3941	Cubic
2	15.750	14.780	5.62199	5.98890	112	0.5750	
3	19.173	30.442	4.62535	2.93395	0–34	0.1835	
4	22.745	31.060	3.90641	2.87697	143	0.8947	
5	27.003	25.007	3.29929	3.55793	322	2.7442	
6	31.953	21.827	2.79862	4.06865	230	0.4726	
7	43.881	29.813	2.06158	2.99445	242	0.0551	

Table 6 X-ray of $[Cu(L)_2(H_2O)_2]Cl_2$**(4d)**

Peak No	Observed 2θ	Calculated 2θ	Observed d	Calculated d	hkl	FWHM	Structure
1	11.312	15.183	7.81620	5.83076	210	0.8727	Hexagonal
2	13.841	13.380	6.39288	6.61207	−212	0.3815	
3	15.341	12.310	5.77105	7.18428	−221	0.4893	
4	18.132	16.739	4.88851	5.29203	−123	0.6387	
5	22.190	23.042	4.00288	3.85669	040	0.5056	
6	26.225	27.084	3.39539	3.28967	006	0.6569	
7	32.103	30.982	2.78589	2.88409	−621	0.5599	

All the complexes of ligand showed the weight loss in the range of 175–225 °C in TG curves, termed as the first stage of thermal degradation. The percentage of weight loss of 8.35–11.24% observed can be attributed to water molecules. The expulsion of water molecule from the complex in the above temperature range indicates that the water molecule is present inside the coordination sphere [49]. The second stage of degradation occurs in the range 250–384 °C, in this stage the percentage of weight loss of 42.81–47.94% is assigned to loss of organic moiety (i.e., ligand **(L)**).

The third stage of weight loss 75.25–81.36% is accomplished in the range 431–568 °C in TG curve of complex are termed as the third stage of thermal decomposition. In this stage, the percentage of weight loss matches the loss of inorganic ligand. The final decomposition product which was left behind above 650 °C corresponds to their respective metal(II)oxide. On the basis of percentage loss in weight, the significant steps of thermal degradation can be formulated.

$$\left[M(L)_2\left(H_2O\right)_2\right]Cl_2 \xrightarrow[-H_2O]{175-225\,^{\circ}C} \left[M(L)_2\right]Cl_2$$

$$\xrightarrow[-L_2]{250-384\,^{\circ}C} [M]Cl_2 \xrightarrow[-Cl_2]{431-568\,^{\circ}C} MO$$

Powder XRD analysis

X-ray diffraction study is useful to elucidate crystal structure of metal complexes. Generally, the crystal structure of a substance determines the diffraction pattern of that substance or more specifically, the shape and size of the unit cell determines the angular positions of the relative intensities of the lines. Since structure determines the diffraction pattern, from the diffraction pattern one can arrive at the structure.

The X-ray diffraction pattern of the complexes $[Ni(L)_2(H_2O)_2]Cl_2$ and $[Cu(L)_2(H_2O)_2]Cl_2$ was recorded between 10 and 70 °C. All the peaks have been indexed, and their $\sin^2\theta$ values was compared with the calculated

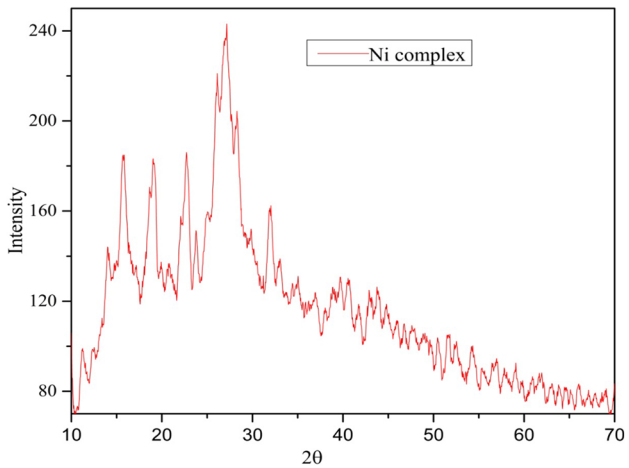

Fig. 6 Powdered XRD of Ni(II) complex **(4c)**

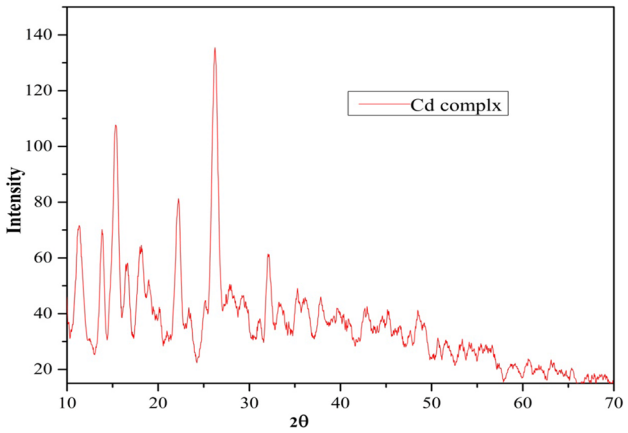

Fig. 7 Powdered XRD of Cu(II) complex (**4d**)

ones, and also the unit cell parameters like a, b, c, α, β, δ have been calculated.

The X-ray diffraction data of the complexes are presented in Tables 5 and 6. The diffractogram records 7 reflections as shown in (Figs. 6 and 7) between 10° and 70° (2θ) with maximum reflection 2θ = 43.881which corresponds to d = 2.0615 A° with hkl values of (242) using wavelength 1.5405 A°. All the peaks have been indexed [50, 51], and their 2θ values were compared with calculated ones, which reveal that there is a good agreement between calculated and observed values of 2θ (Table 5). The unit cell has been determined by the trial error method [52, 53].

The unit parameters obtained for $[Ni(L)_2(H_2O)_2]Cl_2$ are standard deviation (2θ) = 8.7549, average deviation (2θ) = 7.5234 and the cell volume V = 3156.9459.

Substitution of the cell volume in the following formula gives the theoretical value of density equal to 1.7125 g cm^{-3}. For calculating density, we have used the following equations;

$$\text{Density} = n \times M_W / N \times V,$$

Where $n = 6$.

M_W = Molecular weight of the complex,

N = Avagadro's number, 6.023×10^{23}.

V = Cell volume.

Based upon the data, the complex is suggested to be cubic in nature.

The X-ray diffraction pattern of the complexes $[Cu(L)_2(H_2O)_2]Cl_2$ is presented in Figs. 6 and 7. The complex were recorded 7 reflections between 10° and 70° with maximum reflections at 2θ = 11.312 which corresponds to d = 7.8162A°. All the peaks have been indexed [54, 55], and their 2θ values compared with calculated ones, the unit cell parameters are standard deviation (2θ) = 2.0371, average deviation (2θ) = 1.6555 and the cell volume V = 5424.0177.

Based upon the data, the complex is suggested to be hexagonal in nature.

Biological studies

Anti-microbial assay

The biological activities of the synthesized complexes have been investigated to display the possibility of their uses in the bioinorganic and medicinal field. The in vitro antimicrobial activity studied against Gram −ve bacteria as *E. coli* (MTCC 443), *P. aeruginosa* (MTCC 2453) and Gram + ve bacterial strains as *B. subtilis* (MTCC 121) and two fungal strains *Aspergillus flavus (*MTCC 3306*) Candida albicans*(MTCC 3017). This study highly encourages that the metal complexes have higher inhibitory effects than the free ligand. It is evident that the metal coordination tends to make the ligands strong bacteriostatic and fungistatic agents and efficiently inhibits both bacterial cell and mycelia growth of drug-resistant microbes more than the parental ligand. MIC data display varying degrees of biocidal effects of the ligand and its metal complexes on the growth of tested species (Table 7). All of these synthesized compounds showed MIC values in micromolar range (3.02–19.6 µg/ml). Out of these, Ni(II) **(4c)** is the most bioactive (MIC 3.09 µg/ml) against tested gram-negative bacteria compared to standard Ciproflaxcinand Flucanazole. The inhibition values indicate that most complexes have higher percentage toward Gram-negative bacteria compared to Gram positive is due to the metal ions shared with the donor atoms (N and O) of the ligand and the π-electron delocalization over the chelate ring increases electron density over C=N nitrogen leading to strong interactions with cell constituents. The augmented toxicity of metal complexes could be explained on the light of Overtone's concept [56] and Tweedy's chelation theory [57]. As per these theories, the mode of action of the metal complexes may involve the formation of hydrogen bond formation through the azomethine group (HC=N−) with the active centers of cell constituents [58] resulting in interference with the normal cell process [59]. Antimicrobial activity observed in the order Nickel > Copper > Cobalt > Manganese > Ligand.

Antioxidant activity

Human LDL oxidation assay

Oxidation modification is known to play an important role in the pathogenesis of atherosclerosis and coronary heart diseases [60] and the dietary antioxidants that protect LDL from oxidation may therefore reduce atherogenesis and

Table 7 Antimicrobial activity of ligand **(L)** and their metal complexes **4(a–d)**

Sl. No	Compounds	MIC (zone of inhibition ± SD) in ug/ml			
		E. coli	*P. aeruginosa*	*B. subtilis*	*C. albicans*
1	Ligand(3)	11.8 (18 ± 0.6)	12.06 (19 ± 0.5)	12.14 (17 ± 0.6)	19.6 (12 ± 0.2)
2	Mn(II)**(4a)**	4.34 (23 ± 0.3)	4.89 (21 ± 0.4)	4.52 (22 ± 0.4)	12.8 (24. ± 0.5)
3	Co(II) **(4b)**	3.91 (24 ± 0.4)	3.94 (23 ± 0.3)	3.92 (24 ± 0.4)	10.6 (23 ± 0.6)
4	Ni(II) **(4c)**	3.02 (22 ± 0.4)	3.09 (24 ± 0.5)	3.02 (24 ± 0.4)	8.84 (26 ± 0.2)
5	Cu(II) **(4d)**	3.81 (23 ± 0.5)	3.84 (22 ± 0.4)	3.83 (23 ± 0.5)	11.3 (20 ± 0.4)
6	Ciproflaxcin	3.12 (20 ± 0.6)	3.12 (20 ± 0.6)	3.0 (27 ± 0.6)	–
7	Flucanazole	–	–	–	6.25 (16 ± 0.6)

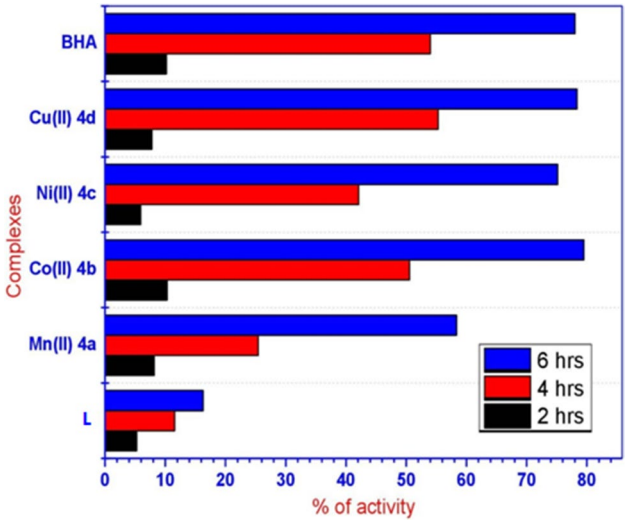

Fig. 8 Percentage LDL oxidation inhibition by ligand **(L)** and their metal complexes **(4a–d)** at 10 µM concentration

coronary heart diseases [61]. In general, oxidation of LDL follows a radical chain reaction that generates conjugated diene hydroperoxides as its initial products. It has been reported that inhibition of human LDL oxidation may arise due to free-radical scavenging [62]. The antioxidant activity of (*Z*)-*N*′((1H-indol-3-yl)methylene)nicotinohydrazide Schiff base **(L)**, and their metal complexes (**4a–d**) against human LDL oxidation with two different concentrations (10 µM and 25 µM) have been studied, and obtained results were showed in the Figs. 8 and 9.

The poly unsaturated fatty acid (PUFA) of human LDL were oxidized, and the malonoldehyde (MDA) formed have been estimated by thiobarbituric acid (TBA) method. The compounds protect LDL from oxidation were measured by the prolongation of the induction time for the formation of conjugated dienes. Initially, ligand **(L)** showed certain degree of activity, further coordination with metal there has been increase in the activity of metal complexes. At the end of 2 h after the induction of oxidation, Co(II) complexes displayed dominant activity compared to other complexes and also standard while exhibiting10.30 and 20.50% protection at 10 and 25 µM levels. Whereas, it was 79.50 and 95.55% protection at the end of 6 h showing dominant inhibition over LDL oxidation and exhibits more activity than the standard drug BHA. The results indicate a dose-dependent inhibition effect of compounds against LDL oxidation. The complexes of Mn(II), Ni(II), Cu(II), after the completion of 6 h exhibited 45.10–78.30% and 85.15–91.50%. In short, we made an attempt to enhance the free radical inhibition effect by different metal complexes.

DNA cleavage

The cleavage of pBR322 plasmid DNA with some synthesized Co(II), Ni(II) and Cu(II) (**4b-d**) complexes in the absence and presence of H_2O_2 as an oxidant has been monitored by agarose gel electrophoresis as shown in Fig. 10. DNA cleavage is controlled by the relaxation of the supercoiled circular form of pBR322 plasmid DNA into the nicked circular form [63], and it was analyzed by monitoring

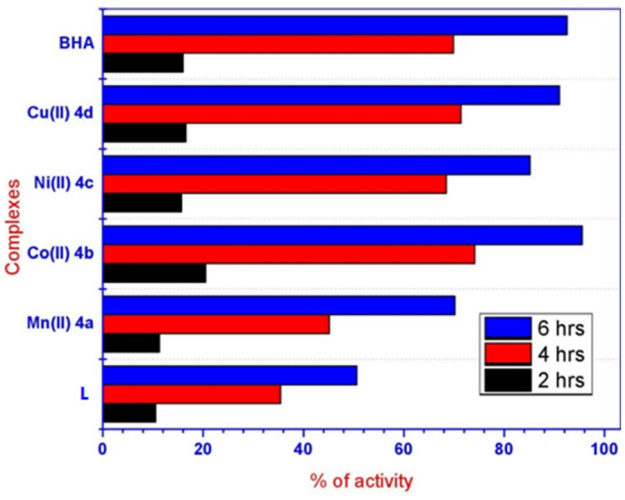

Fig. 9 Percentage LDL oxidation inhibition by ligand **(L)** and their metal complexes **(4a–d)** at 25 µM concentration

Fig. 10 Cleavage of supercoiled pBR322 DNA (0.5 µg) by the Co(II), Ni(II) and Cu(III) complexes in a buffer containing 50 mM Tris–HCl and 50 mM NaCl at 37 °C. Lane 1 DNA alone; Lane 2, DNA + 40 µl of Cobalt complex + H_2O_2; Lane 3,DNA + 40 µl of Cobalt complex; Lane 4, DNA + 60 µl of Cobalt complex; Lane 5, DNA + 40 µl of Nickel complex; Lane 6, DNA + 60 µl of Nickel complex; Lane 7, DNA + 40 µl of Copper complex; Lane 8, DNA + 60 µl of Copper complex Forms I-II are supercoiled and nicked circular DNA, respectively

the conversion of supercoiled DNA (FORM-I) to nicked DNA (FORM-II).To determine the ability of synthesized complexes for DNA scission, the complexes were incubated at different concentrations of 40 µM and 60 µM concentration with Supercoiled pBR322 DNA for 1 h in 50 mM *Tris*–HCl/50 mM NaCl buffer (pH 7.2) [64]. In the absence of the metal complexes, no DNA cleavage was observed for the control [lane 1]. The mechanism of nucloephilic activity of complexes have been investigated. DNA alone(control) does not show activity. In the absence of H_2O_2, observed molecular weight difference in lanes compared to control indicated their partial nucleolytic activity. Probably this may be due to the redox behavior of the metal ion. These results indicate the important role of the metal ions in cleavage studies. In the presence of H_2O_2 with cobalt complex (lane 2), the bands observed indicated the complete DNA cleavage. As a result, in the presence of oxidant, DNA cleavage activity was more than its absence. It may be due to the formation of hydroxyl radicals. The general oxidative DNA cleavage mechanism was proposed in the literature by several research groups [65, 66]. The Fig. 10 shows as the complex concentration increases, the intensity of the circular supercoiled DNA (FORM-I) decreases while that for the nicked (FORM-II) increases. Compounds were observed to cleave the DNA, concludes that the compound inhibit the growth of the pathogenic organism by cleaving the genome.

Conclusion

In this article, the metal complexes of Mn(II), Co(II), Ni(II) and Cu(II) with Schiff base ligand**(L)** derived from indole-3-carboxaldehyde and nicotinic acid hydrazide have been synthesized and characterized. The ligand acts asbidentate coordinates through nitrogen and oxygen atoms of azomethine and carbonyl groups of nicotinic acid hydrazide, respectively. The structures of complexes were confirmed by spectral, analytical, thermal and magnetic studies. The Mn(II), Co(II), Ni(II) and Cu(II) complexes have shown octahedral geometry. The Ni(II) metal complex of the ligand showed good antimicrobial activity. Co(II) complex displayed dominant human LDL oxidation activity compared to other complexes as well as standard at 10 and 25 µM levels. In the Co(II) and Cu(III) complexes, the intensity of the circular supercoiled DNA (FORM-I) decreases while that for the nicked (FORM-II) increases as compared to other complexes, but the cleavage activity is more when H_2O_2 is added as an external oxidizing agent.

Supplementary Information The online version contains supplementary material available at https://doi.org/10.1007/s13738-022-02580-1.

Acknowledgements One of the authors, Ms. Neelufar owes her sincere gratitude to the University Grants Commission (F. No. 16-6(DEC.2017)/2018(NET/CSIR)), New Delhi(India) for the award of Junior Research Fellowship under the UGC-JRF-Fellow.

Declarations

Conflict of interest The authors declare that they have no conflict of interest.

References

1. H.E. Hosseini, M. Mirzaei, S. Zarghami, A. Bauza, A. Frontera, J.T. Mague, M. Habibid, M. Shamsipur, CrystEngComm **16**, 1359–1377 (2014)
2. M. Bazargan, M. Mirzaei, C. Antonio Franconetti, Dalton Trans. **48**, 5476–5490 (2019)
3. V. Sharma, P. Kumar, D. Pathak, J. Heterocycl. Chem. **47**, 491–502 (2010)
4. N.K. Kaushik, N. Kaushik, P. Attri, N. Kumar, C.H. Kim, A.K. Verma, Molecules **18**, 6620–6662 (2013)
5. U. Misra, A. Hitkari, A.K. Saxena, S. Gurtu, K. Shanker, Eur. J. Med. Chem. **31**, 629–634 (1996)
6. A. El-Gendy Adel, A.N. Abdou, Z.S. El-Taher, A.H. El-Banna, Alex. J. Pharm. Sci. **7**, 99–103 (1993)
7. N. Karali, A. Gürsoy, F. Kandemirli, Bioorg. Med. Chem. **15**, 5888–5904 (2007)
8. Z.H. MasoudMirzaei, A. Jafari, P. Hosseinpour, M.D. Yousefi, RSC Adv. **9**, 25382–25404 (2019)
9. A.S. Kalgutkar, B.C. Crews, S. Saleh, D. Prudhomme, L.J. Marnett, Bioorg. Med. Chem. **24**, 6810–6822 (2005)
10. I.A. Leneva, N.I. Fadeeva, I.T. Fedykina, Eur. J. Med. Chem. **33**, 143–148 (1994)
11. E.R. El-Sawy, F.A. Bassyouni, S.H. Abu-Bakr, H.M. Rady, M.M. Abdlla, Acta Pharm. **60**, 55–71 (2010)
12. E.R. El-Sawy, A.H. Mandour, M. Khaled, I.E. Islam, H.M. Abo-Salem, Acta. Pharm. **62**, 157–179 (2012)
13. A.Y. Merwade, S.B. Rajur, L.D. Basanagoudar, Ind. J. Chem. B **12**, 1113–1117 (1990)
14. A.E. Fernandez, V.A. Monge, Span. Patent Chem. Abstr. **83**, 400–436 (1975)
15. N. Ergenç, N.S. Günay, R. Demirdamar, Eur. J. Med. Chem. **33**, 143–148 (1998)
16. O. Kahn, Acc. Chem. **33**, 647–657 (2000)
17. A.D. Huters, K.W. Quasdorf, E.D. Styduhar, K.N. Garg, J. Am. Chem. Soc. **133**, 15797–15799 (2011)

18. H.B. Jackson, J. Org. Chem. **29**, 1158–1160 (1964)
19. T. Nagasaka, S. Ohki, Chem. Pharm. Bull. **25**, 3023–3033 (1977)
20. H.B. Jackson, J. Org. Chem. **32**, 4095–4098 (1967)
21. C. Ali, U. Serhan, S. Mehmet, J. Saudi Chem. Soc. **22**, 757–766 (2018)
22. S. Dong, G. Yan, J. Yanxing, Angewandte Chem. Int. Ed. **52**, 4902–4906 (2013)
23. Z. Shafiq, Z. Qiao, L. Liu, Q.Y. Zheng, D. Wang, Y.J. Chen Tunable, E. Thiem, J. Synlett. **18**, 2965–2969 (2009)
24. Z. Shafiq, L. Liu, Z. Liu, D. Wang, Y.J. Chen, ACS Publ. Org. Lett. **9**, 2525–2528 (2007)
25. M. Mirzaei, H. Eshtiagh-Hosseini, Z. Karrabi, K. Molcanov, E. Eydizadeh, J.T. Mague, A. Bauzad, A. Frontera, CrystEngComm **16**, 5352–5363 (2014)
26. B. Zou, C. Chen, S.Y. Leong, M. Ding, P.W. Smith, Tetrahedron Lett. **70**, 578–582 (2014)
27. M. Mirzaei, H. Eshtiagh Hosseini, A. Bauza, S. Zarghami, CrystEngComm **16**, 6149–6158 (2014)
28. J.M. Matthews, M.N. Greco, L.R. Hecker, Bioorg. Med. Chem. Lett. **13**, 753–756 (2003)
29. G. Mohammadnezhada, H. Farrokhpour, H. Gorls, W. Plass, J. Mol. Struct. **1230**, 12985 (2021)
30. G. Mohammadnezhad, O. Akintola, A. Buchholz, H. Gorls, W. Plass, New. J. Chem. **43**, 45 (2019)
31. H.E. Hosseini, M. Mirzaei, M. Biabani, V. Lippolis, M. Chahkandi, C. Bazzicalupi, CrystEngComm **15**, 6752 (2013)
32. A. Kulkarni, S.A. Patil, P.S. Badami, Eur. J. Med. Chem. **44**, 2904 (2009)
33. N. Shahid, N. Sami, M. Shakir, M. Aatif, J. Saudi Chem. Soc. **23**, 315–324 (2019)
34. M. Mirzaei, H. Eshtiagh Hosseini, M. Shamsipur, M. Saeedi, RSC Adv. **5**, 72923–72936 (2015)
35. M. Bazargan, M. Mirzaei, M. Aghamohamadi, M. Tahmasebi, J. Mol. Struct. **1202**, 127243 (2020)
36. K.H. KumarNaik, S. Selvaraj, N. Nagaraja, SpectrochimicaActa Part A Mol. Biomol. Spectrosc. **131**, 599–605 (2014)
37. N. Naik, K.H. Kumar, SpectrochimicaActa Part A Mol. Biomol. Spectrosc. **141**, 88–93 (2015)
38. I. Wiegand, K. Hilpert, R.E.W. Hancock, Nat. Prot. **2**, 163–175 (2008)
39. M.S. Surendra Babu, P.G. Krishna, K. Hussain Reddy, G.H. Philip, Main Group Chem. **8**, 101–114 (2009)
40. V. Tamilarasan, N. Sengottuvelan, A. Sudha, P. Srinivasan, G. Chakkaravarthi, J. Photochem. Photobiol. **162**, 558–569 (2016)
41. W.J. Geary, Coord. Chem. Rev. **7**, 81 (1971)
42. M.R. Gill, H. Derrat, C.G.W. Smythe, G. Battaglia, J.A. Tomas, Chem. Bio. Chem. **12**, 877–880 (2011)
43. T. Mehmet, K. Huseyin, S.M. Kasim, S. Selahattin, Trans. Metal Chem. **24**, 414 (1999)
44. R.M. Patil, M.M. Prabhu, Int. J. Chem. Sci. **8**, 52–58 (2010)
45. S. Prema, A. Pasupathy, S.R. Bheeter, Int. J. Sci. Res. Publ. **6**, 721–723 (2016)
46. K.I. Alexopoulou, E. Zagoraiou, T.F. Zafropoulos, SpectrochimicaActa Part A Mol. Biomol. Spectr. **136**, 122–130 (2015)
47. V. Gomathi, R. Selvameena, Asia. J. Chem. **25**, 2083–2086 (2013)
48. D.P. Singh, K. Kumar, C. Sharma, SpectrochimicaActa Part A Mol. Biomol. Spectr. **75**, 98–105 (2010)
49. A.V. Nikolaev, V.A. Logvieka, L.I. Mychina, J. Therm. Anal., Acadmia press, New Yok. **2,** 779 (1969)
50. J.R. Carvajal, R.T. Winplotr, A Graphic Tool For Powder Diffraction, Laboratoire Leon Brilloiun, Gifsur Yvette Cedex. France. **2**, 198 (2004)
51. D.P. Shoemaker, C.W. Garland, *Eeperiments in physical chemistry*, vol. 17, 5th edn. (McGraw-Hill International Edition, New York, 1989), pp. 179–182
52. M.J. Buerger, *X-ray crystallography*, vol. 100 (John Wiley and sons, New York, 1953), pp. 6–7
53. G. Mohammadnezhad, R. Debel, W. Plass, J. Mol. Catal. A Chem. **410**, 160–167 (2015)
54. H. Peiser, H.P. Rooksey, A.J.C. Wilson, in *X-Ray Diffraction by Polycrystalline Materials*, vol 344 (Institute of Physics, London, 1956), pp. 201–206
55. S.W. Chin-hua, R.G. Rossman, H.B. Gray, G.S. Hammond, J.H. Schugar, Inorg. Chem. **11**, 10 (1972)
56. U.V. Arndt, D.C. Creagh, R.D. Deslattes, J.H. Hubbel, P. Indelicato, E.G. Kessler, Int. Tables X-Ray Crystallogr **75**, 191–258 (2006)
57. Y. Anjaneyulu, R.P. Rao, Synth React. Inorg. Metal-Org Nano-Metal Chem. **16**, 257–272 (1986)
58. L. Mishra, V.K. Singh, Ind. J. Chem. **32**, 446–457 (1993)
59. L. Malhotra, S. Kumar, K.S. Dhindsa, Ind. J. Chem. **32A**, 457–459 (1993)
60. R.V. Patel, S.W. Park, Res Chem. Intermed. **41**, 5599–5609 (2015)
61. D. Teinberg, S. Parthasarathy, T.E. Carew, J.C. Khoo, J.L. Witztum, N. Engl, J. Med. **320**, 915–927 (1989)
62. J.E. Kinsella, E. Frankel, B. German, Kanner J. Food Technol. **47**, 85–93 (1993)
63. E.A. Decker, V. Ivanov, B.Z. Zhu, B.J. Frei, Agric. Food Chem. **49**, 511 (2001)
64. P. Jayaseelan, S. Prasad, S. Vedanayaki, R. Rajavel, Arab. J. Chem. **9**, S668–S677 (2016)
65. K.R. Sangeetha Gowda, H.S. BhojyaNaik, B. Vinay Kumar, C.N. Sudhamani, H.V. Sudeep, T.R. RavikumarNaik, G. Krishnamurthy, Spectrochim. Acta Part A **105**, 229–237 (2013)
66. R. Gup, O. Erer, N. Dilek, J. Mol. Struct. **1129**, 142–151 (2017)